Faraday Discussions

On the Mechanism of Intermolecular Nitrogen-Atom Transfer from a Lattice-Isolated Diruthenium Nitride Intermediate

Journal:	*Faraday Discussions*
Manuscript ID	FD-ART-11-2022-000167.R1
Article Type:	Paper
Date Submitted by the Author:	16-Dec-2022
Complete List of Authors:	Cosio, Mario; Texas A&M University, Chemistry Alharbi, Waad ; University of North Texas Sur, Aishanee; Texas A&M University, Chemistry Wang, Chen-Hao; Texas A&M University, Chemistry Najafian, Ahmad; University of North Texas Cundari, Thomas; University of North Texas, Chemistry Powers, David; Texas A&M University, Chemistry

On the Mechanism of Intermolecular Nitrogen-Atom Transfer from a Lattice-Isolated Diruthenium Nitride Intermediate

Mario N. Cosio,[#,1] Waad S. Alharbi,[#,2,3] Aishanee Sur,[1] Chen-Hao Wang,[1] Ahmad Najafian,[2] Thomas R. Cundari,[2,*] and David C. Powers[1,*]

[#]authors contributed equally to this work
[1]Department of Chemistry, Texas A&M University, College Station, Texas 77843-3255, USA
[2]Department of Chemistry, Center of Advanced Scientific Computing and Modeling (CASCaM), University of North Texas, 1155 Union Circle, #305070, Denton, Texas 76203-5017, USA
[3]Chemistry Department, Science College, University of Jeddah, Jeddah, KSA.
Correspondence: thomas.cundari@unt.edu, powers@chem.tamu.edu

Abstract

Catalyst confinement within microporous media provides the opportunity to site isolate reactive intermediates, enforce intermolecular functionalization chemistry by co-localizing reactive intermediates and substrates in molecular-scale interstices, and harness non-covalent host-guest interactions to achieve selectivities that are complementary to those accessible in solution. As part of an ongoing program to develop synthetically useful nitrogen-atom transfer (NAT) catalysts, we have demonstrated intermolecular benzylic amination of toluene at a Ru_2 nitride intermediate confined within the interstices of a Ru_2-based metal-organic framework (MOF), $Ru_3(btc)_2X_3$ (btc = 1,3,5-benzenetricarboxylate, *i.e.*, Ru-HKUST-1 for X = Cl). Nitride confinement within the extended MOF lattice enabled intermolecular C–H functionalization to benzylic C–H bonds in preference to nitride dimerization, which was encountered with soluble molecular analogues. Detailed study of the kinetic isotope effects (KIEs, *i.e.*, k_H/k_D) of C–H amination, assayed both as intramolecular effects using partially labeled toluene and as intermolecular effects using a mixture of per-labeled and unlabeled toluene, provided evidence for restricted substrate mobility on the time scale of interstitial NAT. Analysis of these KIEs as a function of material mesoporosity provided approximate experimental values for functionalization in the absence of mass transport barriers. Here, we disclose a combined experimental and computational investigation of the mechanism of NAT from a Ru_2 nitride to the C–H bond of toluene. Computed kinetic isotope effects for a H-atom abstraction (HAA) / radical rebound (RR) mechanism are in good agreement with experimental data obtained for C–H amination at the rapid diffusion limit. These results provide the first detailed analysis of the mechanism of intermolecular NAT to a C–H bond, bolster the use of KIEs as a probe of confinement effects on NAT within MOF lattices, and provide mechanistic insights unavailable by experiment because rate-determining mass transport obscured the underlying chemical kinetics.

Introduction

Confinement of catalysts within porous media provides opportunities to site isolate reactive species, stabilize catalytic intermediates,[1] and utilize non-bonding interactions between the pore space and the substrate to engender selectivity that is complementary to solution-phase catalysts.[2, 3] As an example, confinement effects have been leveraged to impact selectivity between reaction pathways that differ in activation volume.[4,5] From a practical perspective,

immobilization of catalysts within a porous support provides opportunities in catalyst recycling by facilitating catalyst re-isolation as well as improved catalyst durability.[6-9] In order to leverage the myriad potential opportunities conferred by confinement effects, detailed understanding of the diffusional processes by which substrates enter interstitial reactions spaces and by which products escape is required.

Restricted diffusivity of guest molecules in a porous material is expected if the pore size of the material is similar or smaller than the root-mean-square path length of the same guest molecule in its pure state.[10] For common organic small molecules (diameter < 1 nm), restricted diffusion is expected in micro- and lower mesoporous materials (pore size < 10 nm).[11, 12] Additionally, tortuosity (*i.e.,* how twisted a pore is)[13, 14] and effective transport-through porosity (*i.e.,* a measure of pores that are not terminated with closed ends)[15] can also further suppress substrate diffusivity in porous catalysts.

The restricted diffusivity of organic small molecules in microporous lattices impacts the development and efficiency of MOF catalysis: the catalyst turnover frequency (TOF) of reactions that confront mass transport barriers (*i.e.*, confined diffusion) is suppressed relative to an idealized reaction that proceeds without mass transport limitations. The relationship between catalytic activity and particle size of porous catalysts has been famously described by a parameter known as the Thiele modulus.[16] Two limiting cases of the Thiele modulus are : 1) a regime in which the reaction rate is limited by the inherent turnover frequency of the catalysts (*i.e.*, a system free of diffusional restrictions), and 2) a regime in which the reaction rate is limited by substrate diffusion to the active site.[17] An effectiveness factor can also be calculated by dividing the observed reaction rate by the inherent reaction rate (*i.e.*, turnover frequency (TOF) of a non-diffusionally restricted active site).[18] In essence, this effectiveness factor symbolizes how many of the total catalytic sites in a porous material are utilized (*i.e.*, active). The Thiele modulus/effectiveness factor is a macroscopic measure (*i.e.*, a measure of bulk flux) of diffusion and should be compared to microscopic measurements (*i.e.*, tracking an average of individual molecules), such as pulsed field gradient NMR experiments,[12] to ensure consistency.[18]

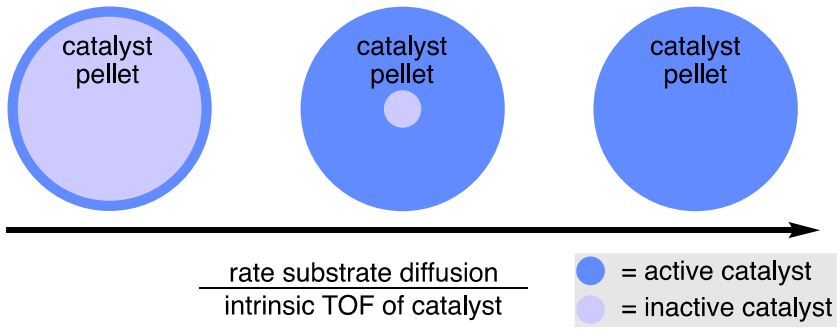

Figure 1. The intrinsic catalyst turnover frequency (TOF) is inherently coupled to the portion of active sites that engage in catalysis in porous media. When the catalyst TOF is significantly higher than diffusional processes, only catalyst sites at or near the particle surface are active. When the catalyst TOF is significantly lower than diffusional processes, most or all interstitial catalyst sites are active.

Our group has a long-standing interest in developing NAT reactions as a complement to well-developed nitrogen-group transfer (NGT) chemistry.[19, 20] NAT chemistry would proceed at a metal-supported atomic nitrogen ligand (*i.e.*, metal nitrides, nitridyls, or nitrenido intermediates) as opposed to the nitrene intermediates that characterize NGT chemistry. NGT introduces both nitrogen content and one *N*-substituent in a pairwise fashion.[21] Thus, the *N*-substituent directly impacts the reactivity and selectivity with which the incipient metal nitrenoid engages substrate. NAT provides a conceptual framework to decouple the introduction of these two motifs. For NAT, the nitrogen content is installed by reaction of a metal nitride with a C–H bond and the *N*-substituent is installed in a subsequent reaction step, *e.g.*, the electrophilic cleavage of the M–N bond in the metal amide intermediate. Compared to NGT reactions,[22-26] NAT chemistry is underdeveloped. Potential obstacles to the development of NAT chemistry are bimolecular nitride dimerization to liberate N_2 and the proclivity of reactive nitrides to engage in deleterious unimolecular reactions with oxidatively labile sites on the ancillary ligand set (*e.g.*, weak C–H bonds or nucleophilic donor atoms).

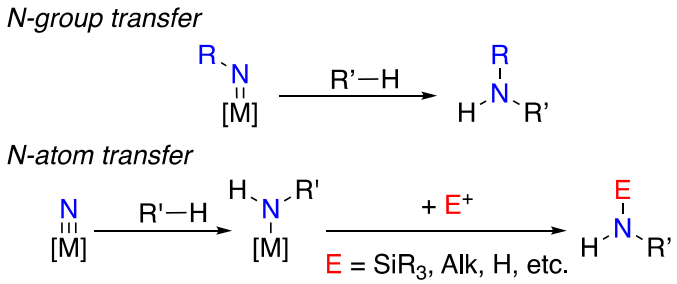

Figure 2. Comparison of the synthetic disconnections implicit in nitrogen-group transfer (NGT) and nitrogen-atom transfer (NAT) schemes.

Inspired by the work of Berry *et al.*, who reported a transient formamidinate-supported molecular Ru_2 nitride effected aromatic C–H amination at cryogenic temperatures (Figure 3), [27-29] we sought to site isolate Ru_2 nitrides within a porous material in which sites of potential oxidative lability were systematically removed. Our studies focused on reaction chemistry in a Ru_2-based MOF assembled by polymerization of 1,3,5-benzenetricarboxylic acid with $Ru_2(OAc)_4Cl$.[30, 31] Installation of lattice supported Ru_2N_3 sites was achieved by soaking the Ru_2Cl-based materials with NaN_3 in DMF/H_2O. NAT to benzylic C–H bonds was then achieved by thermolysis of toluene impregnated Ru_2N_3-based materials followed by acidic workup. Benzylamine was the sole *N*-containing organic small molecule that was detected from this reaction sequence. To probe the mechanism of NAT in the materials, we evaluated the KIE for C–H amination. When measured with d_1-toluene (*i.e.*, intramolecular KIE), a k_H/k_D = 7.86(3) was measured, which is consistent with a HAA-initiated reaction to generate benzylamine. In contrast, when measured using a mixture of d_8- and d_0-toluene (*i.e.*, intermolecular KIE), the k_H/k_D = 1.02(2). We attributed the difference between these two values to be a consequence of substrate confinement in the Ru-HKUST-1 material, which limits the diffusion of the substrate in the pores. The low intermolecular KIE value may indicate an increase in substrate "stickiness" due to restricted diffusion in the confined material. This is consistent with the lack of observed KIE in enzymatic systems where substrate commitment to the catalyst is high.[32] In a later report

we synthesized a series of increasingly defective materials[33, 34] (and therefore increasingly mesoporous materials) to modulate substrate confinement in the Ru-HKUST-1 system, using intra- and intermolecular KIE measurements as a probe for confinement.[20] We observed a near convergence of intra- and intermolecular KIE values in the most mesoporous systems (Figure 4c). However, experimental extrapolation to the diffusionally unrestricted regime was not possible because isostructural materials were not available with sufficient mesoporosities.

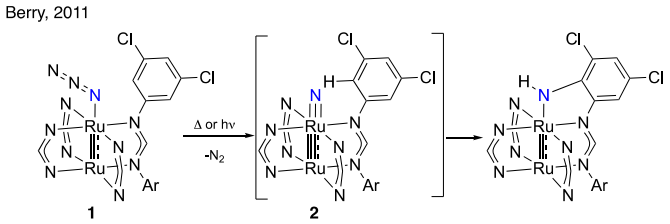

Figure 3. Intramolecular C(sp^2)–H amination from formamidinate-bridge Ru_2 nitride **2**.

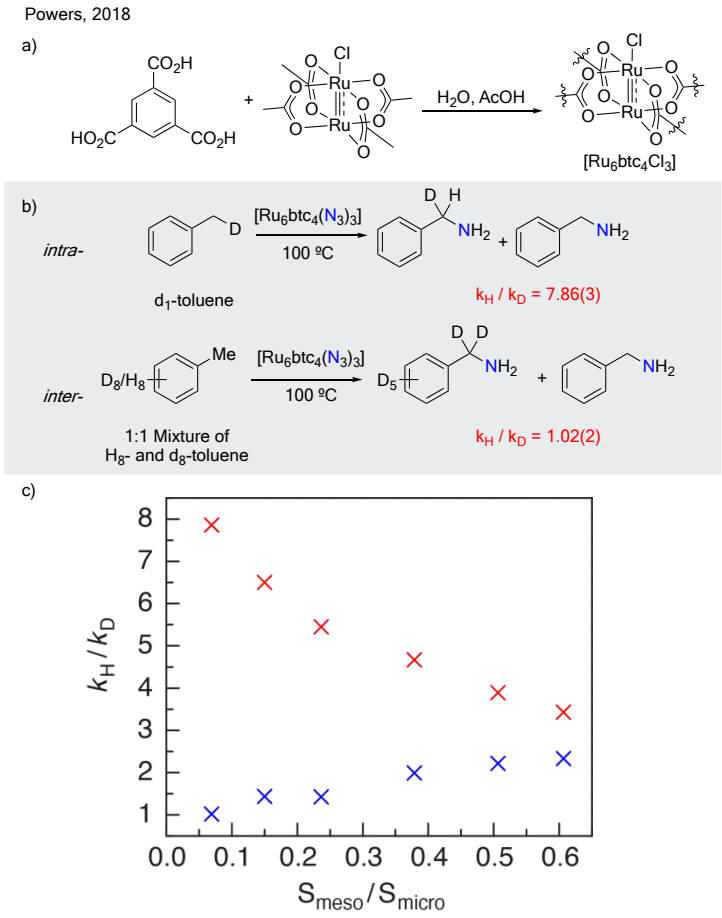

Figure 4. a) Polymerization of $Ru_2(OAc)_4Cl$ with 1,3,5-benzenetricaboxylic acid results in formation of $[Ru_6btc_4Cl_3]$ (Ru-HKUST-1) b) Comparison of intra- and intermolecular KIEs (top and bottom, respectively) for toluene amination indicate that substrate diffusion is slow relative to NAT.[19, 20] c) The intramolecular KIE decreases with increasing mesoporosity and the intermolecular KIE increases with mesoporosity.[20] These data suggest that the diffusional restrictions responsible for the disparate KIEs in the microporous materials are relaxed as the pore size increases.

While our initial studies provided significant experimental evidence for restricted substrate mobility during NAT, questions regarding the mechanism of C–N bond construction remained unanswered. First, the mechanistic origin of the disparate reactivity of the Ru_2 nitride described by Berry *et al.*, which engages in C(sp^2)–H amination,[29] and the tetracarboxylate-bridged sites in our materials, which engage in selective benzylic C–H amination,[19] was unresolved. Second, our analysis of the impact of material porosity on the observed kinetic isotope effects suggested that in the absence of mass transport limitations the KIEs would be identical regardless of the isotopic labeling pattern of the substrate. These questions are challenging to address experimentally, not least of which because many common methods of characterization of solid materials are unavailable in the Ru_2(II,III) materials under discussion: Due to the S = 3/2 ground state of the Ru_2[II,III] moieties and the lack of accessible single-crystals of Ru-HKUST-1, solid-state NMR and single crystal X-ray diffraction experiments are hard to implement.[35] Pulsed Field Gradient NMR has been used in porous systems as a microscopic measure of diffusion; however, this method relies on the ability to generate large single crystalline materials,[36] which has thus far proven elusive for the materials under consideration. Further, while a number of NAT reactions with C–H bonds have been reported,[22,37-42] the molecular analogue of our previously reported tetracarboxylate Ru_2 nitride is unstable in solution,[19] which prevents study of molecular models of NAT. Consequently, we turned our attention to using kinetic isotope effect (KIE) experiments as a probe of the relative rates of substrate mobility and functionalization.

Here, we report a Density Functional Theory (DFT) investigation of NAT from a Ru_2 nitride to a C–H bond. The results of this investigation point to NAT via HAA/radical rebound at a doublet Ru_2 nitride intermediate. In addition, the computed mechanism reproduces both the observed chemoselectivity for benzylic C–H functionalization over potential aromatic C–H amination and the KIE data obtained from experiments on the most mesoporous, and thus least confined, materials currently available.

Results

A. Experimental and Computational Characterization of Ru_2 Azide and Nitrides

In order to evaluate the chemistry in this motif and to provide an experimental benchmark for computational work, we sought to synthesize and characterize a molecular Ru_2N_3 supported by bridging carboxylate ligands.

Ru_2 Azides. Treatment of Ru_2(esp)$_2$Cl with sodium azide results in clean replacement of the chloride ligand with an azide (esp = α,α,α′,α′-tetramethyl-1,3-benzenedipropionic acid, Figure 5). Support for complete ligand exchange was obtained by IR spectroscopy and powder X-ray diffraction (PXRD) (Figures S2 and S3).

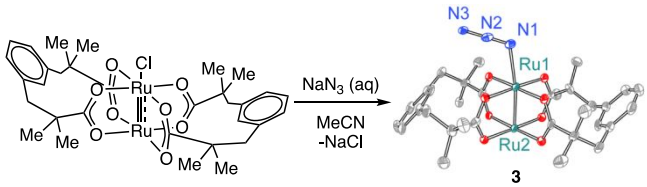

Figure 5. Synthesis and X-ray structure of **3**. Displacement ellipsoid plot drawn at 50% probability. H-atoms are omitted for clarity

Single crystals of Ru_2 azide **3** were obtained by concentrating a DMF solution of **3** and the metrical parameters obtained by refinement of the X-ray diffraction data are collected in Table 1. Of note, the Ru_2–N bond distance (2.230(7) Å) is much longer than that previous observed in formamidinate-supported complex **1** (2.042(4) Å). Geometry optimization of both formate- and benzoate-bridged Ru_2 azide complexes were carried out: the identity of the bridging ligand had little impact on the resulting Ru_2 azide structure. The optimized structures differed strongly from the crystallographically determined metrics of **3** (data are collected in Table 1). Examination of the crystal packing of **3** revealed that the Ru_2N_3 motif in **3** catenates as $–M_2X–$ chains in the solid state via Ru–N bonds to both ends of the azide ligand. Differences in electronic structure of esp vs. benzoate as well as Lewis acid activation (via the axial site on a second Ru_2 center) may be the cause of this variation; thus, esp-bridged Ru_2 azide **3** does not provide a faithful model of the isolated Ru_2N_3 sites in Ru-HKUST-1.

Table 1. Comparison of experimental and computed metrics for $Ru_2(esp)_2N_3$ and $Ru_2(OBz)_4N_3$.

	$Ru_2(esp)_2N_3$ (**3**), Expt.	$Ru_2(OBz)_4N_3$, Calc.
Ru(1)–Ru(2) / Å	2.230(7)	2.347
Ru(1)–N(1) / Å	2.2870(9)	2.203
Ru(2)–Ru(1)–N(1) / °	170.5(2)	175.6

Ru_2 Nitrides. The tetracarboxylate-bridged Ru_2 nitride that we ascribe amination activity to in $[Ru_4(btc)_6(N_3)_3]$ is transient and has not been observed experimentally. The closest analogue that has been experimentally evaluated is formamidinate-bridged complex **1**, which has been characterized in the solid state by EPR, EXAFS, and photocrystallography (metrics are collected in Table 2).

Consistent with available experimental and computational data for the formamidinate-bridged diruthenium nitride, carboxylate-bridged nitride **3** is calculated to display an $S = ½$ ground state with the unpaired spin occupying the Ru–Ru δ orbital. The optimized geometry calculated for **3** is in good agreement with the experimentally defined structure of the formamidinate-bridged analogue (Table 2). The computed Ru nitride bond length 1.651 Å (benzoate-bridged model) is longer than the median bond length (1.60 Å, 54 examples) obtained from Ru nitrides extracted from the Cambridge Crystallographic Database, which are largely mono-metallic species. One may thus infer that the second Ru, trans to the Ru-nitride bond, infers some nitridyl (N^{2-}) character to the active species and a reduction in the ruthenium-nitrogen bond order, which is consistent with a strong structural trans effect of the distal Ru center. This analysis is further supported by the substantial spin calculated for the nitridyl radical ($r_{spin} = –0.4\ e^–$).

Table 2. Comparison of metrical parameters in experimentally determined nitride **2** and geometry optimized nitride **4**.

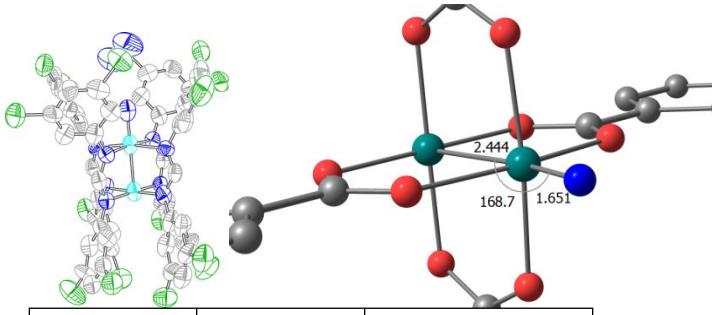

	2, Expt.	**4**, Calc.
Ru–Ru (Å)	2.408(3)	2.444
Ru–N (Å)	1.72(2)	1.651
Ru–Ru–N (°)	180	168.7

B. Mechanisms of C–H Amination

To gain insight into the mechanism of C–H amination at lattice-confined Ru_2 nitrides motifs, a DFT analysis was pursued of toluene amination via a diruthenium nitride intermediate. We based our study on previously reported pathways for oxidation chemistry from high-valent metal oxo complexes[43,44] as well as pathways for electrophilic aromatic substitution.[27,45-46, 47] Based on these precedents, we considered four reaction mechanisms: 1) benzylic amination via initial hydrogen-atom abstraction to generate a formally Ru_2(II,IV) imide and an organic radical, which is then followed by rebound to afford a metal benzylamide intermediate, 2) an analogous two-step sequence to accomplish amination of the aromatic C–H bond *para* to the methyl substituent of toluene via the intermediacy of an aryl radical (Figure 6a), 3) electrophilic aromatic substitution via a Wheland-type intermediate to accomplish aromatic C–H amination (Figure 6b), and 4) electrophilic aromatic substitution (EAS) via an azirido intermediate (Figure 6c). We evaluated both the potential energy surfaces (PESs) of these processes as well as computed relevant k_H/k_D values to compare with experimental data.

Among the mechanisms studied, a tetrahedral Wheland-type intermediate (Figure 6b) collapsed to the azirido intermediate (Figure 6c) upon geometry optimization. Moreover, the transition state (TS) for 1,2-hydrogen migration was higher (by 3.6 kcal/mol) than the initial electrophilic attack TS; computed KIE values for both transition states along the EAS pathways yielded $k_H/k_D \sim 1$, which is inconsistent with experiment. Both TSs in the EAS pathways were also considerably higher than the transition state for benzylic C–H activation, Figure 7. The TS for activation of the arene C–H bond trans to the methyl substituent of toluene was also much higher than the benzylic C–H activation TS ($\Delta\Delta G^{\#}$ = 18.5 kcal/mol). Hence, our discussion focuses on the pathway indicated by DFT to be favored energetically, *i.e.*, benzylic C–H activation followed by radical rebound. As will be seen, this pathway also has a calculated KIE that is consistent with experiment. Details on the other pathways are included in Supporting Information.

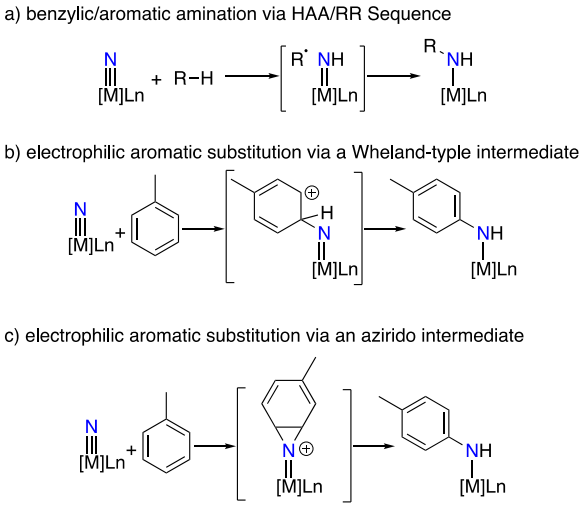

Figure 6. Summary of potential reaction mechanisms that have been evaluated for NAT from a lattice-confined Ru_2N site to toluene to afford a Ru_2 amide. The mechanisms that have been evaluated are (a) stepwise H-atom abstraction / radical rebound processes at either the benzylic or aromatic C–H bond, (b) electrophilic substitution via a Wheland intermediate, or (c) electrophilic substitution via an azirido intermediate.

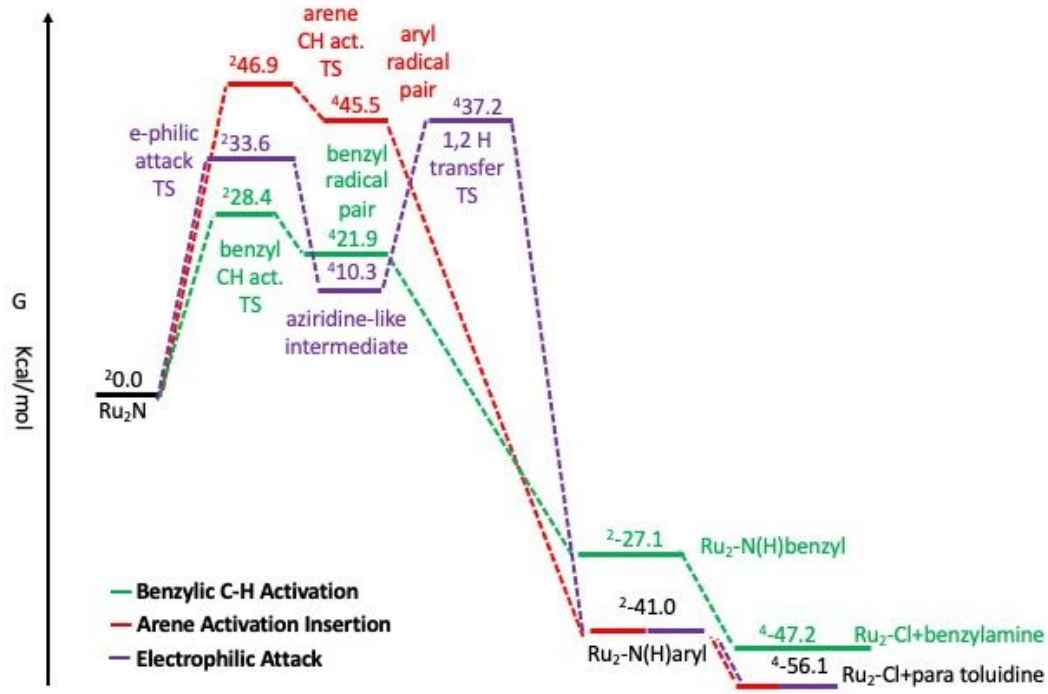

Figure 7. DFT computed reaction coordinate (free energies in kcal/mol relative to separated reactants) for toluene activation by different pathways HAA benzylic (green), HAA aromatic (red), electrophilic aromatic substitution, aziridine-like (purple). The numerical prefix denotes the computed lowest-energy spin state for that particularly stationary state.

Benzylic C–H Amination via an H-atom abstraction (HAA)/radical rebound (RR) mechanism. The free energy surface for activation of a benzylic C–H bond of toluene via nitrogen insertion is illustrated in Figure 7. Benzoate-bridged diruthenium nitride (**Ru_2N**) engages in H-atom

abstraction via a doublet TS to afford a radical pair intermediate, which is comprised of a formally Ru[II,IV] imido complex and a benzyl radical (ΔG_{rel} = 21.9 kcal/mol versus separated **Ru_2N** + toluene). The latter is a doublet organic radical, and the former inorganic radical is a triplet for a total spin of S = $^3/_2$ for the pair. The metrics of the HAA TS are characterized by contraction of the Ru–Ru bond from 2.444 to 2.413 Å, elongation of the Ru–N bond from 1.651 to 1.766 Å, and a slight linearization of the Ru–Ru–N angle from 168.7° to 169.4° (Figure 8). The benzylic C–H activation TS is 28.4 kcal/mol higher in free energy than nitride. Radical rebound combines the benzyl radical and the Ru_2[II,IV] imide to generate a Ru_2 benzylamide complex via a highly exergonic reaction (ΔG = –27.1 kcal/mol for **Ru_2N** + toluene = Ru_2-N(H)benzyl). Making the reasonable assumption that the barrier for the highly exergonic radical rebound step is negligible, benzylic C-H activation was deemed to have the lowest free energy rate-determining step calculated in this work.

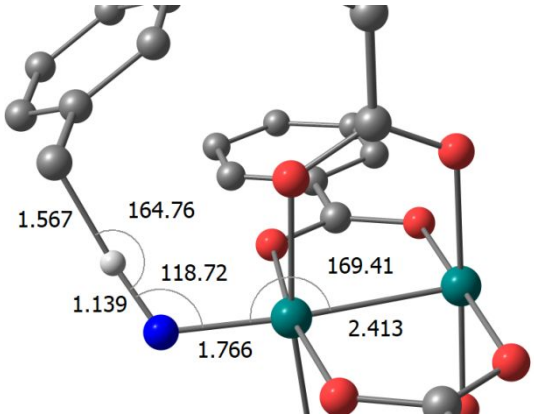

Figure 8. DFT computed transition state benzylic activation of toluene. Bond lengths in Å, bond angles in degrees.

Using the rate-determining transition state for benzylic HAA, a k_H/k_D = 3.85 at 100 °C was computed. This KIE is consistent with the significant C–H cleavage that is evident in the HAA transition state (Figure 7) and is consistent with experimental estimates for the intrinsic KIE for toluene amination at tetracarboxylate-bridged Ru_2N motifs in the absence of mass transport barriers (*vide infra*).

Discussion

The conceptual analogy of MOF interstices to enzyme active sites has motivated enormous interest in the design, synthesis, and application of MOF-based materials as catalysts in fine-chemical synthesis. While enormous synthetic effort has resulted in the rapid development of new materials for catalysis,[48, 49] the development of kinetic tools to evaluate those new materials have been slow to emerge.[10, 50]

Our laboratory has been broadly interested in the development of new selective methods to enable conversion of C–H bonds to synthetically valuable *N*-containing organic small molecules.[19, 20, 51, 52] The bulk of successfully implemented C–H amination methods rely on nitrogen-group transfer (NGT) and effect conversion of C–H to C–N(H)R products in which the identity of the *N*-substituent R is dictated by the structure of the reactive nitrene intermediate. [22-26] We have been attracted to nitrogen-atom transfer (NAT) as a complementary synthetic platform for amination

in which C–H amination at a metal nitride affords metal amide intermediates that could be readily diversified via a subsequent functionalization event (*e.g.*, electrophilic cleavage, etc.).

Realization of synthetically useful NAT chemistry requires access to reactive metal nitrides and the development of strategies to achieve *intermolecular* NAT events. To this end, we have been inspired by 1) the reports by Berry *et al*. that diruthenium nitrides engage in cryogenic intramolecular NAT chemistry, and 2) the improved stability of lattice-confined active sites towards bimolecular decomposition (a common decomposition pathway for electrophilic nitrides)[53-57] and 3) the potential to use confinement effects within Ru_2-based porous materials to engender intermolecular NAT to substrates confined within lattice interstices. In 2018, we demonstrated a single-turnover synthetic cycle for the conversion of toluene to benzylamine upon thermolysis of a toluene-impregnated Ru_2N_3-based material.[19] We attributed the observed intermolecular chemistry to non-covalent co-localization of the reactive nitride and the toluene substrate. During mechanistic studies of these reactions, we noted a striking difference in the magnitude of the kinetic isotope effect for toluene amination that depended on whether the KIE was determined using an intra- or intermolecular H/D probe.

The difference between the intra- and intermolecular KIEs (7.86(3) vs. 1.02(2)) is consistent with significant mass transport barriers during interstitial NAT. While the intramolecular KIE reflected the expected kinetic preference for C–H vs. C–D cleavage, the lack of an intermolecular KIE effect revealed the rate determining step was mass transport not functionalization: Group transfer proceeded more quickly than solvent exchange within the pores of our MOF material. To further evaluate the hypothesis that mass transport limitations were the source of divergence between the intra- and intermolecular KIEs, we subsequently interrogated the impact of material mesoporosity on the magnitude of intra- and intermolecular KIEs. Consistent with this model, increasing mesoporosity indeed led to convergence of the respective KIEs. *Because the kinetics for these reactions were convoluted with mass transport, further understanding of the mechanism of the NAT step was unavailable from experiment.*

To gain further insight into the intimate details of NAT, we evaluated both stepwise HAA / RR based mechanisms and electrophilic substitution processes. Calculations were benchmarked against the crystallographically defined structures of **1** and **3** and the photocrystallographically determined structure of **2**. The lowest-barrier process for NAT that was identified proceeded via HAA / RR at the benzylic C–H bond of toluene. This mechanism is consistent with the observed exclusive benzylic amination products with no aryl C–H amination detected. Using the potential energy surface for benzylic HAA / RR, we calculated a k_H/k_D = 3.8 at 100 °C. Re-examination of the mesoporosity-dependent KIEs indicated that at the limit of high mesoporosity the intra- and intermolecular KIEs converge to ~3. The close agreement between this value and that calculated for benzylic C–H abstraction is consistent with the absence of mass transport barriers at high mesoporosity: At sufficiently large pore size, solvent self-exchange becomes fast relative to group transfer from a diruthenium nitride (Figure 9).

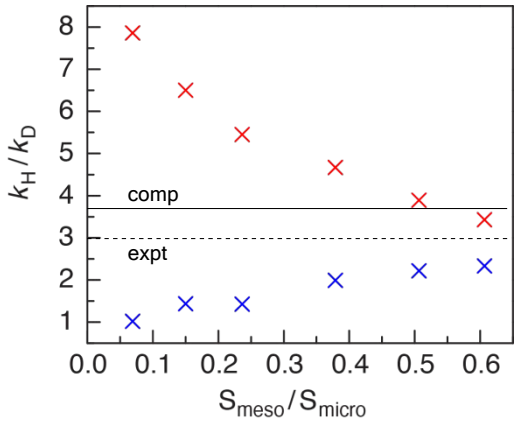

Figure 9. Re-examination of the porosity-dependent KIEs for NAT to toluene. The KIE calculated for the HAA/RR pathway (3.8) is in good agreement with the apparent convergence of inter- and intramolecular KIEs (~3).

Finally, the KIEs in the most and least mesoporous samples included in Figure 4c showed disparate behavior as a function of temperature: the most mesoporous materials behaved classically while the most confined sample displayed significant temperature dependence. While classical explanations for large kinetic isotope effects have been suggested for HAT events to M=E bonds,[58] given the mesoporosity-sensitive temperature dependence, we speculated that confinement induced tunneling during C–H cleavage was responsible for enhancement of the intrinsic KIE in microporous materials. This hypothesis garners support from our current computational work: The computed KIE suggests that the larger KIEs observed in the microporous materials arise from factors that are not accounted for in molecular-level calculations. Confinement effects are non-innocent with respect to this kinetic parameter. The observed porosity-dependent tunneling is analogous to tunneling proposed for HAA reactions in a family of lipoxygenase enzymes with systematically tuned active site volumes.[59]

Conclusion

In conclusion, here we described a detailed experimental and computational analysis of NAT at a tetracarboxylate-bridged Ru_2 nitride intermediate. The results are consistent with an HAA/radical rebound pathway via the intermediacy of a benzylamide and a Ru_2(II,IV) imido species. The computed mechanism reproduces the experimental data for amination in the least confined materials that are synthetically accessible.

These results also highlight the critical role of theory and experiment in evaluating mechanisms in porous materials. While the analysis of KIEs has been widely used in the analysis of molecular organometallic catalysis, the approach has challenges when employed to study confined systems: The inability to experimentally deconvolute mass-transport and reaction barriers can complicate the analysis of experimentally obtained KIEs. In the present experiments, experimental definition of the mesoporosity-dependent kinetic behavior, coupled with the atomistic model from DFT computations, clarifies the origins of the observed chemical kinetics. These results demonstrate that while confinement is a powerful tool to improve and modulate reactivity, methods to study reactions free of confinement may be equally valuable.

Acknowledgements

D.C.P. and M.N.C. acknowledge the U.S. Department of Energy (DOE), Office of Science, Office of Basic Energy Sciences, Catalysis Program (DE-SC0018977) and the Welch Foundation (A-1907). T.R.C. and W.S.A. acknowledge the U.S. Department of Energy, Office of Science, Basic Energy Sciences (DE-FG02- 03ER15387) for their support of this research. T.R.C. and W.S.A. also thank the Saudi Arabian Cultural Mission in the USA for their support of W.S.A.

References

1. C. Copéret, *Pure Appl. Chem.*, 2009, **81**, 585-596.
2. U. Pindur, G. Lutz and C. Otto, *Chem. Rev.*, 1993, **93**, 741-761.
3. J. Liu, T. A. Goetjen, Q. Wang, J. G. Knapp, M. C. Wasson, Y. Yang, Z. H. Syed, M. Delferro, J. M. Notestein, O. K. Farha and J. T. Hupp, *Chem. Soc. Rev.*, 2022, **51**, 1045-1097.
4. A. Dewaele, B. Van Berlo, J. Dijkmans, P. A. Jacobs and B. F. Sels, *Catal. Sci. Technol.*, 2016, **6**, 2580-2597.
5. E. Pump, Z. Cao, M. K. Samantaray, A. Bendjeriou-Sedjerari, L. Cavallo and J.-M. Basset, *ACS Catal.*, 2017, **7**, 6581-6586.
6. W. Wang, L. Cui, P. Sun, L. Shi, C. Yue and F. Li, *Chem. Rev.*, 2018, **118**, 9843-9929.
7. M. P. Conley, C. Copéret and C. Thieuleux, *ACS Catal.*, 2014, **4**, 1458-1469.
8. X. S. Zhao, X. Y. Bao, W. Guo and F. Y. Lee, *Mater. Today*, 2006, **9**, 32-39.
9. P. Balla, P. K. Seelam, R. Balaga, R. Rajesh, V. Perupogu and T. X. Liang, *J. Environ. Chem. Eng.*, 2021, **9**, 106530.
10. W.-Y. Gao, A. D. Cardenal, C.-H. Wang and D. C. Powers, *Chem. Eur. J.*, 2019, **25**, 3465-3476.
11. P. Grathwohl, *Diffusion in natural porous media: contaminant transport, sorption/desorption and dissolution kinetics*, Springer Science & Business Media, 2012.
12. T. M. Osborn Popp, A. Z. Plantz, O. M. Yaghi and J. A. Reimer, *ChemPhysChem*, 2020, **21**, 32-35.
13. F. Elwinger, P. Pourmand and I. Furó, *J. Phys. Chem. C*, 2017, **121**, 13757-13764.
14. E. E. Petersen, *AIChE Journal*, 1958, **4**, 343-345.
15. D. A. Lever, M. H. Bradbury and S. J. Hemingway, *J. Hydrol.*, 1985, **80**, 45-76.
16. E. W. Thiele, *Ind. Eng. Chem.*, 1939, **31**, 916-920.
17. B. A. Johnson, A. M. Beiler, B. D. McCarthy and S. Ott, *J. Am. Chem. Soc.*, 2020, **142**, 11941-11956.
18. D. M. Ruthven, in *Stud. Surf. Sci. Catal.*, eds. J. Čejka, H. van Bekkum, A. Corma and F. Schüth, Elsevier, 2007, vol. 168, pp. 737-785.
19. C.-H. Wang, A. Das, W.-Y. Gao and D. C. Powers, *Angew. Chem. Int. Ed.*, 2018, **57**, 3676-3681.
20. C.-H. Wang, W.-Y. Gao and D. C. Powers, *J. Am. Chem. Soc.*, 2019, **141**, 19203-19207.
21. M. N. Cosio and D. C. Powers, *Nat. Rev. Chem.*, 2022, Submitted.
22. J. L. Roizen, M. E. Harvey and J. Du Bois, *Acc. Chem. Res.*, 2012, **45**, 911-922.
23. K. Shin, H. Kim and S. Chang, *Acc. Chem. Res.*, 2015, **48**, 1040-1052.
24. J. R. Clark, K. Feng, A. Sookezian and M. C. White, *Nat. Chem.*, 2018, **10**, 583-591.
25. H. Lu and X. P. Zhang, *Chem. Soc. Rev.*, 2011, **40**, 1899-1909.
26. R. Singh and A. Mukherjee, *ACS Catal.*, 2019, **9**, 3604-3617.

27. A. K. M. Long, G. H. Timmer, J. S. Pap, J. L. Snyder, R. P. Yu and J. F. Berry, *J. Am. Chem. Soc.*, 2011, **133**, 13138-13150.
28. J. S. Pap, S. DeBeer George and J. F. Berry, *Angew. Chem. Int. Ed.*, 2008, **47**, 10102-10105.
29. A. K. Musch Long, R. P. Yu, G. H. Timmer and J. F. Berry, *J. Am. Chem. Soc.*, 2010, **132**, 12228-12230.
30. O. Kozachuk, K. Yusenko, H. Noei, Y. Wang, S. Walleck, T. Glaser and R. A. Fischer, *Chem. Commun.*, 2011, **47**, 8509-8511.
31. C. R. Wade and M. Dincă, *Dalton Trans.*, 2012, **41**, 7931-7938.
32. G. T. Miwa, J. S. Zweig, J. S. A. Walsh and A. Y. H. Lu, in *Microsomes, Drug Oxidations and Chemical Carcinogenesis*, eds. M. J. Coon, A. H. Conney, R. W. Estabrook, H. V. Gelboin, J. R. Gillette and P. J. O'Brien, Academic Press, 1980, DOI: https://doi.org/10.1016/B978-0-12-187701-9.50071-1, pp. 363-366.
33. O. Kozachuk, I. Luz, F. X. Llabrés i Xamena, H. Noei, M. Kauer, H. B. Albada, E. D. Bloch, B. Marler, Y. Wang, M. Muhler and R. A. Fischer, *Angew. Chem. Int. Ed.*, 2014, **53**, 7058-7062.
34. W. Zhang, M. Kauer, O. Halbherr, K. Epp, P. Guo, M. I. Gonzalez, D. J. Xiao, C. Wiktor, F. X. Llabrés i Xamena, C. Wöll, Y. Wang, M. Muhler and R. A. Fischer, *Chem. Eur. J.*, 2016, **22**, 14297-14307.
35. G. R. Lorzing, K. P. Balto, A. M. Antonio, B. A. Trump, C. M. Brown and E. D. Bloch, *Chem. Mater.*, 2020, **32**, 7710-7715.
36. C. L. Cavalcante, Jr. and D. M. Ruthven, *Ind. Eng. Chem. Res.*, 1995, **34**, 185-191.
37. H. Henning, K. Hofbauer, K. Handke and R. Stich, *Angew. Chem. Int. Ed.*, 1997, **36**, 408-410.
38. J. Schöffel, N. Šušnjar, S. Nückel, D. Sieh and P. Burger, *Eur. J. Inorg. Chem.*, 2010, **2010**, 4911-4915.
39. C. C. Hojilla Atienza, A. C. Bowman, E. Lobkovsky and P. J. Chirik, *J. Am. Chem. Soc.*, 2010, **132**, 16343-16345.
40. W.-L. Man, W. W. Y. Lam, H.-K. Kwong, S.-M. Yiu and T.-C. Lau, *Angew. Chem. Int. Ed.*, 2012, **51**, 9101-9104.
41. J. Xie, W.-L. Man, C.-Y. Wong, X. Chang, C.-M. Che and T.-C. Lau, *J. Am. Chem. Soc.*, 2016, **138**, 5817-5820.
42. J. Xiang, X.-X. Jin, Q.-Q. Su, S.-C. Cheng, C.-C. Ko, W.-L. Man, M. Xue, L. Wu, C.-M. Che and T.-C. Lau, *Commun. Chem.*, 2019, **2**, 40.
43. X. Huang and J. T. Groves, *J. Biol. Inorg. Chem.*, 2017, **22**, 185-207.
44. B. Wilkinson, M. Zhu, N. D. Priestley, H. H. T. Nguyen, H. Morimoto, P. G. Williams, S. I. Chan and H. G. Floss, *J. Am. Chem. Soc.*, 1996, **118**, 921-922.
45. G. Koleva, B. Galabov, J. Kong, H. F. Schaefer and P. v. R. Schleyer, *J. Am. Chem. Soc.*, 2011, **133**, 19094-19101.
46. W. F. Trager, in *Comprehensive Medicinal Chemistry II*, eds. J. B. Taylor and D. J. Triggle, Elsevier, Oxford, 2007, DOI: https://doi.org/10.1016/B0-08-045044-X/00119-X, pp. 87-132.
47. B. Li, Y. Li, Y. Dang and K. N. Houk, *ACS Catal.*, 2021, **11**, 6816-6824.
48. H. Xiong, Y. Dong, D. Liu, R. Long, T. Kong and Y. Xiong, *J. Phys. Chem. Lett.*, 2022, **13**, 1272-1282.
49. B. Szczęśniak, J. Choma and M. Jaroniec, *Chem. Commun.*, 2020, **56**, 7836-7848.

50. D. Yang and B. C. Gates, *ACS Catal.*, 2019, **9**, 1779-1798.
51. H. Tan, S. Samanta, A. Maity, P. Roychowdhury and D. C. Powers, *Nat. Commun*, 2022, **13**, 3341.
52. P. Roychowdhury, R. G. Herrera, H. Tan and D. C. Powers, *Angew. Chem. Int. Ed.*, 2022, **61**, e202200665.
53. W.-L. Man, T.-M. Tang, T.-W. Wong, T.-C. Lau, S.-M. Peng and W.-T. Wong, *J. Am. Chem. Soc.*, 2004, **126**, 478-479.
54. K. D. Demadis, T. J. Meyer and P. S. White, *Inorg. Chem.*, 1997, **36**, 5678-5679.
55. H.-W. Lam, C.-M. Che and K.-Y. Wong, *J. Chem. Soc., Dalton Trans.*, 1992, DOI: 10.1039/DT9920001411, 1411-1416.
56. S. V. Park, A. R. Corcos, A. N. Jambor, T. Yang and J. F. Berry, *J. Am. Chem. Soc.*, 2022, **144**, 3259-3268.
57. O. Krahe, E. Bill and F. Neese, *Angew. Chem. Int. Ed.*, 2014, **53**, 8727-8731.
58. L. M. Slaughter, P. T. Wolczanski, T. R. Klinckman and T. R. Cundari, *J. Am. Chem. Soc.*, 2000, **122**, 7953-7975.
59. T. Jonsson, M. H. Glickman, S. Sun and J. P. Klinman, *J. Am. Chem. Soc.*, 1996, **118**, 10319-10320.